Journal of Applied Toxicology

WILEY

Journal of AppliedToxicology

RESEARCH ARTICLE OPEN ACCESS

Occupational Exposure to Factory-Derived Particulate Matter 2.5 Induces Cutaneous Toxicity in Workers and HaCaT Keratinocytes Through Oxidative Stress and Inflammation

Miku Tanaka[1] | Masayuki Takaishi[1,2] | Iroha Okuda[3] | Toshiki Fujimoto[1] | Mayumi Tsuji[4] | Yuri Okano[5] | Yasuhiro Ishihara[3] | Maori Kono[1,2]

[1]Advanced Technology Institute, Mandom Corporation, Osaka, Japan | [2]Laboratory of Advanced Cosmetic Science, Graduate School of Pharmaceutical Sciences, Osaka University, Osaka, Japan | [3]Program of Biomedical Science, Graduate School of Integrated Sciences for Life, Hiroshima University, Hiroshima, Japan | [4]Department of Environmental Health, School of Medicine, University of Occupational and Environmental Health, Fukuoka, Japan | [5]CIEL Co. Ltd., Sagamihara, Kanagawa, Japan

Correspondence: Maori Kono (maori.kono@mandom.com)

Received: 19 September 2025 | **Revised:** 18 November 2025 | **Accepted:** 20 November 2025

Keywords: cutaneous toxicity | inflammation | keratinocytes | occupational exposure | oxidative stress | PM2.5 | skin barrier dysfunction | welding fumes

ABSTRACT

This study aimed to evaluate the toxicological effects of occupational exposure to factory-derived particulate matter (PM2.5) on human skin, emphasizing its role as a potential target organ of environmental toxicants. An epidemiological survey comparing factory and nonfactory workers was conducted by assessing their skin elasticity and color on the neck and forehead. Carbonylated proteins and inflammatory cytokines were quantified using tape stripping, and stratum corneum (SC) desquamation and cell area were analyzed using Brilliant Green staining. In addition, HaCaT keratinocytes were exposed to factory-derived PM2.5 (welding fumes), and oxidative stress, inflammation, and barrier function were assessed using gene expression analysis and reporter assays. Factory workers showed reduced dermal elasticity, increased skin redness, elevated levels of carbonylated proteins and inflammatory cytokines (IFN-γ and CXCL10), and enhanced SC desquamation with smaller cell areas. Consistently, in vitro exposure of HaCaT keratinocytes to PM2.5 induced oxidative stress (activation of the antioxidant response element pathway), inflammatory responses (nuclear factor kappa B activation), and suggested barrier impairment. These findings reveal that chronic occupational exposure to welding fumes impairs skin structure and function through oxidative stress, inflammation, and barrier disruption, highlighting the skin as a relevant target organ in occupational toxicology.

1 | Introduction

Airborne pollutants, especially fine particulate matter (PM2.5), induce oxidative stress and inflammatory responses in the skin (Piao et al. 2018; Dijkhoff et al. 2020; Hu et al. 2017). They are also well known to contribute to respiratory, neurological, and inflammatory airway diseases (Wang et al. 2015; Yu et al. 2022; Yue et al. 2023; Ishihara et al. 2019; Tanaka et al. 2023). The cutaneous effects of these pollutants include barrier disruption (Li et al. 2017; Kim et al. 2023), accelerated skin aging, and increased pigmentation (Ei et al. 2025; Huang et al. 2022; Yang et al. 2022).

Skin condition is commonly evaluated using multiple biophysical parameters, such as stratum corneum (SC) integrity, epidermal elasticity, and hydration. In addition, skin color provides a useful and objective indicator of overall skin health. Changes in these skin conditions are often quantified through objective colorimetric analysis using the CIE L*a*b* color space, where L* represents skin lightness, a* denotes the red–green axis (with higher values indicating erythema), and b* denotes the yellow–blue axis (with higher values indicating yellowness). This system provides a standardized and reproducible method to evaluate pigmentation and redness objectively in both clinical and field studies.

The skin serves as a direct target of PM2.5 exposure, and our previous studies examined the effects of urban traffic-related air pollution on skin condition using three-dimensional (3D) skin models and keratinocyte-based in vitro systems (Kono, Ishihara, et al. 2024; Kono et al. 2023).

In addition to PM2.5, smaller ultrafine particles (UFPs; $< 0.1\,\mu m$) have attracted increasing attention because of their larger surface area-to-mass ratios and stronger biological reactivity. These nanoscale particles can penetrate skin appendages, accumulate within the dermis, and enter systemic circulation, thereby exacerbating oxidative and inflammatory stress (Bocheva et al. 2023; Dijkhoff et al. 2020).

Among UFP sources, welding fumes are particularly relevant, as they comprise both fine (0.1–1 μm) and ultrafine fractions enriched in transition metals such as Fe, Mn, Zn, and Ti. Our previous characterization of welding fumes revealed a predominance of Fe and Mn, metals known to catalyze reactive oxygen species formation (Kono, Ishihara, et al. 2024), indicating that the specific elemental composition of welding-derived particles plays a key role in their stress-inducing and pro-inflammatory potential.

Although in vitro models help elucidate molecular responses and toxicological mechanisms, they cannot fully replicate the complexity of human skin responses under real-world conditions. Notably, epidemiological approaches are essential for understanding the skin effects of PM2.5 exposure in workplaces, where exposure levels are higher and more consistent. Recognizing the skin as a direct target organ in occupational toxicology is critical for comprehensive risk assessment (Bocheva et al. 2023; Chan et al. 2025; Huls et al. 2016). However, discrepancies remain between the findings from experimental models and those observed in human populations.

To address this gap, we focused on occupational settings with relatively well-defined exposure sources and high PM2.5 concentrations, specifically, metal processing factories producing welding fumes. We compared the skin conditions of workers in high-exposure environments with those of nonfactory (office) workers in low-exposed occupational environments. In addition, we conducted in vitro keratinocyte experiments using factory-derived PM2.5 (welding fumes) to assess the underlying molecular mechanisms. Collectively, this integrated approach enables consistent interpretation of structural and molecular responses to PM2.5 exposure and provides insights for developing future skincare interventions against airborne pollutant-induced skin damage.

2 | Materials and Methods

2.1 | Participants and Environmental Exposure Assessment

Participants working in occupational environments with varying levels of PM2.5 exposure were selected, which included adult male metal welders (aged 20–54 years; mean ± standard deviation [SD], 37.2 ± 12.1; $n = 18$) and adult male nonindustrial workers (aged 24–51 years; mean ± SD, 35.9 ± 7.9; $n = 28$). The study protocol was approved by the Ethics Committee of the University of Occupational and Environmental Health, Japan (Approval No. R2-011; Date: February 15, 2024). All participants were informed of the study objectives, procedures, potential risks, and benefits and provided written informed consent before the commencement of the study.

PM2.5 concentrations were measured in the working environment of metal-welding factories in April 2023 and in nonfactory office environments in July 2024, using a portable particle counter (KC-51; Rion Co., Tokyo, Japan) for sizes ranging from 0.3–0.5, 0.5–1, and 1–5 μm. Assuming a spherical geometry, the total particle volume (VE, μm^3) was calculated using the geometric mean diameter (D) for each size range, as described by Kono, Takaishi, et al. 2024:

$$\mathrm{VE}\left(\mu m^3\right) = 4\pi\left\{(\mathrm{N}0.3-0.5)\cdot(\mathrm{D}0.3-0.5)^3 + (\mathrm{N}0.5-1)\cdot(\mathrm{D}0.5-1)^3 + (\mathrm{N}1-5)\cdot(\mathrm{D}1-5)^3\right\}/3$$

where N_{p-q} represents the particle count for the size range p–q μm and D_{p-q} represents the corresponding geometric mean diameter. The density of PM2.5 was set to 1.60 g/cm^3 (Herath et al. 2022). Airborne mass concentration (M, $\mu g/m^3$) per 0.283 L of air was calculated according to Kono, Takaishi, et al. 2024 as follows:

$$\mathrm{M} = (1.60 \cdot \mathrm{VE} / 0.283) \cdot 1000$$

2.2 | Skin Condition Assessment and Sample Collection

All skin measurements were performed without face washing or acclimatization. The viscoelastic properties of the right lateral neck skin were measured using a Cutometer MPA580 (Courage + Khazaka; Cologne, Germany) with 2- and 6-mm probes. A single-cycle suction mode (Mode 1) was used, consisting of a 2-s suction at −450 mbar followed by 2 s of relaxation. Each site was measured five times, and the mean value was used for the analysis. The recorded parameters included the maximum distension (Uf) and immediate retraction ratio (Ur/Uf). The Cutometer outputs were expressed as absolute values (Ua, Ue, Uf, and Uv) and relative parameters (R0–R9) (Figure 1). In this study, R0 (skin pliability), R2 (gross elasticity), R5 (net elasticity), R6 (portion of viscoelasticity), and R7 (immediate recovery) were analyzed (Fujimoto et al. 2023; Ryu et al. 2008; Woo et al. 2014).

Skin color parameters (L*, a*, and b*) were measured at the forehead and neck using a spectrophotometer (CM-600d; Konica Minolta, Tokyo, Japan). Three measurements were obtained

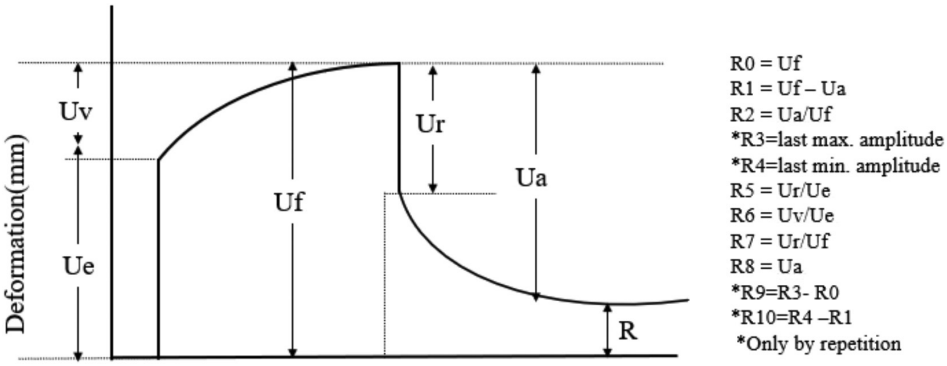

FIGURE 1 | Skin deformation curve constructed using a cutometer and R parameters. The Cutometer records vertical skin deformation induced by negative pressure and its recovery after suction release. The curve shows the immediate distension (Ue), delayed distension (Uv), final deformation (Uf), and recovery (Ur, Ua). Next, mechanical parameters were calculated: R0 (Uf) = maximum deformation, R2 (Ua/Uf) = gross elasticity ratio, R5 (Ur/Ue) = net elasticity ratio, and R7 (Ur/Uf) = biological elasticity ratio.

at each site, and the mean value was used for analysis. In this system, L* indicates skin lightness, a* represents the red–green component (higher values indicate increased erythema), and b* represents the yellow–blue component (higher values indicate increased yellowness).

SC samples were collected noninvasively from the forehead using a standard transparent adhesive tape (Nichiban No. 31B; Tokyo, Japan). After applying pressure for 10 s, three consecutive tape strips were removed from the same site. The first strip was stained with Brilliant Green (BG) and imaged using a fluorescence microscope (BZ-X800; Keyence, Osaka, Japan). The corneocyte area and desquamation index were quantified using dedicated corneocytometry software.

A portion of the second strip was stained with 50-μM fluorescein-5-thiosemicarbazide in 3-(*N*-morpholino)propanesulfonic acid buffer, and the fluorescence intensity of carbonylated proteins was quantified using image analysis using a fluorescence microscope (BZ-X800; Keyence, Osaka, Japan) (Iwai et al. 2010). Another 1 × 1 cm section of the same strip was immersed in phosphate-buffered saline (–) containing 0.05% nonfluorescent Triton X-100. Following centrifugation at 12,000 × *g* for 10 min, the supernatant was collected for cytokine measurements using the ProcartaPlex Human Cytokine Panel (Thermo Fisher Scientific, Waltham, MA, USA). Cytokine concentrations were determined using the Bio-Plex 200 system (Bio-Rad, Hercules, CA, USA) and normalized to the total protein content measured by optical density (Kono et al. 2023).

2.3 | Collection and Preparation of Welding Fume PM2.5

Factory-derived PM2.5 (welding fumes) samples were collected during active metal processing using a high-volume air sampler (HV-500R; Shibata Scientific Technology Ltd., Tokyo, Japan), equipped with high-efficiency polytetrafluoroethylene membrane filters (pore size: 0.2 μm). The filters were stored in sterile containers and immersed in sterile distilled water. The PM2.5 was dispersed by ultrasonication for 20 min and concentrated through centrifugation. The pellet was resuspended to the target concentration of 10 mg/mL and stored at −80°C. The physicochemical properties of the welding fume PM2.5 samples were characterized as described previously (Kono, Ishihara, et al. 2024). Particle morphology and size distribution were analyzed using scanning electron microscopy equipped with energy-dispersive X-ray spectroscopy (SEM–EDX), and elemental composition was determined by inductively coupled plasma–mass spectrometry (ICP–MS) (Table S1). PM2.5 mass concentrations were determined gravimetrically based on filter weights before and after sampling, and the results were cross-checked with particle number–based estimations to ensure measurement consistency.

2.4 | Cell Culture and In Vitro Exposure Procedures

HaCaT human keratinocytes were cultured in Dulbecco's Modified Eagle Medium (DMEM) supplemented with 10% fetal bovine serum and 1% penicillin–streptomycin at 37°C in a humidified 5% CO_2 incubator. Cells were seeded into 96- or six-well plates and treated with fume suspensions at concentrations of 10, 50, and 100 μg/mL for 6 or 24 h. Following exposure, cell viability was assessed by measuring lactate dehydrogenase (LDH) release into the culture medium using a commercially available LDH Cytotoxicity Detection Kit (Roche Diagnostics, Basel, Switzerland) according to the manufacturer's instructions. Absorbance was measured at 490 nm using a microplate reader, and relative cytotoxicity was calculated as a percentage of the total LDH release from lysed cells. Subsequent analyses, including total RNA extraction, luciferase reporter, thiobarbituric acid-reactive substances (TBARS), and Bio-Plex assays, were performed based on the experimental endpoint.

2.5 | Evaluation of NF-κB/ARE Pathway Activation and Downstream Molecular Responses

To assess transcriptional activation of nuclear factor kappa B (NF-κB) and antioxidant response element (ARE) pathways, HaCaT keratinocytes were cotransfected with pGL4.32[luc2P/NF-κB-RE/Hygro] or pGL4.37[luc2P/ARE/Hygro] reporter

vectors (Promega, Madison, WI, USA), and the firefly luciferase-encoding normalization vector pNL1.1.PGK[Nluc/PGK], using Lipofectamine 2000 (Invitrogen, Carlsbad, CA, USA). After 18 h, the cells were replated and fume suspensions were applied approximately 42 h posttransfection for 6 or 24 h.

Luciferase activity was measured using the Dual-Luciferase Reporter Assay System (Promega, Madison, WI, USA) following the manufacturer's protocol. NanoLuc and firefly luciferase signals were quantified using a GloMax luminometer (Promega), and transcriptional activity was calculated as the firefly-to-NanoLuc activity ratio.

For gene expression analysis, total RNA was extracted using the Maxwell RSC SimplyRNA Tissue Kit (Promega) and reverse-transcribed using the SuperScript IV VILO Master Mix (Thermo Fisher Scientific, Waltham, MA, USA). Quantitative polymerase chain reaction (qPCR) was performed using β-actin as the endogenous control, and relative expression levels were calculated using the 2^-ΔΔCt method. The conditioned medium was collected and stored at −80°C until analysis. Cytokine and chemokine levels were determined using the same multiplex immunoassay method as described for the SC samples (ProcartaPlex Human Cytokine Panel; Thermo Fisher Scientific, Waltham, MA, USA) with quantification on a Bio-Plex 200 system (Bio-Rad, Hercules, CA, USA). Evaluation of TBARS levels was estimated as previously described (Ishihara et al. 2012) and were used as an index of lipid peroxidation.

2.6 | Statistical Analysis

Statistical analyses were conducted using GraphPad Prism (version 10; GraphPad Software, San Diego, CA, USA) according to data distribution and experimental design, using appropriate parametric or nonparametric tests (Student's *t*-test, Welch's *t*-test, Mann–Whitney *U* test, one- or two-way analysis of variance (ANOVA) with post hoc tests). Statistical significance was set at $p < 0.05$.

3 | Results

3.1 | Assessment of PM2.5 Exposure in Different Working Environments

Airborne particle numbers were measured at three locations—the welding area in a metal processing factory (Site A), adjacent nonwelding area (Site B), and control site in a nonwelding environment (Site C). For particle sizes of approximately 0.3–0.5, 0.5–1.0, and 1.0–5.0 μm, the counts at Site A were 96,004 ± 2785, 8170 ± 72, and 228 ± 20, respectively; at Site B, they were 43,620 ± 592, 4711 ± 153, and 20 ± 8, respectively; and at Site C, they were 55 ± 5, 11 ± 4, and 1, respectively. The highest particle numbers were observed at Site A. Based on these counts, the calculated mass concentrations at Sites A, B, and C were 112.0 ± 1.3 μg/m^3, 62.6 ± 1.9 μg/m^3, and 0.14 ± 0.08 μg/m^3, respectively (Figure 2). Notably, both Sites A and B exceeded the Japanese environmental standard for the daily mean PM2.5 concentration (35 μg/m^3).

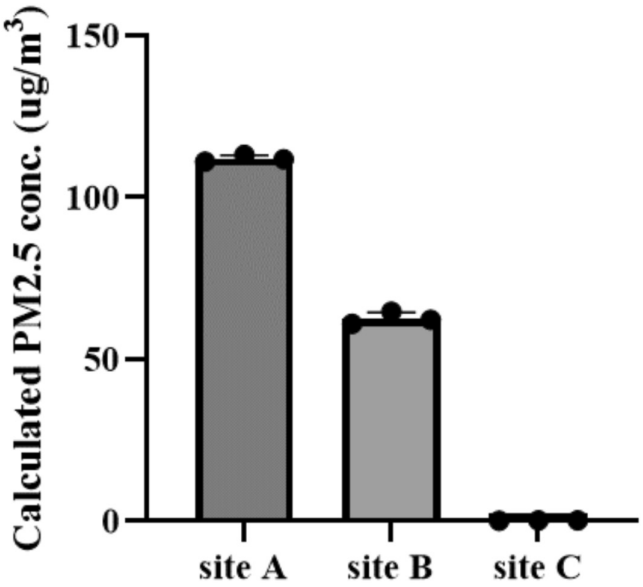

FIGURE 2 | Particle size distribution in the welding area (Site A), adjacent nonwelding area (Site B), and control site (Site C). Data are presented as the mean ± SEM ($n = 3$).

3.2 | Assessment of Skin Condition and Biomarkers

Based on the environmental measurements, workers from Sites A and B ($n = 9$ each) were categorized as the high-exposure group ($n = 18$), and those from Site C as the low-exposure group ($n = 28$).

Skin viscoelasticity was measured using a cutometer with 2- (epidermis-dominant) and 6-mm (dermis-proximal) probe measurements, assessing R0 (skin pliability), R2 (gross elasticity), R5 (net elasticity), R6 (portion of viscoelasticity), and R7 (immediate recovery).

For the 2-mm probe, only R0 significantly differed between the low- and high-exposure groups, showing lower skin pliability in the high-exposure group. For the 6-mm probe, all viscoelastic parameters except R2 showed significant differences, with the high-exposure group exhibiting higher R0 and lower R5–R7 values, thus indicating decreased dermal elasticity and recovery ability (Table 1).

Skin color was measured on the neck and the forehead, evaluating L* (lightness), a* (redness), and b* (yellowness). At the forehead, the a* value was significantly higher in the high-exposure group, indicating increased redness, whereas L* and b* did not differ between the groups. At the neck, a* was also significantly higher in the high-exposure group, whereas L* and b* showed no significant differences (Table 2).

In the high-exposure group, BG staining of SC samples obtained from the forehead showed significantly smaller corneocyte areas and higher multilayered desquamation scores (Figure 3). In addition, the fluorescence ratio of carbonylated proteins, an oxidative stress marker, was significantly higher in the high-exposure group (Figure 4).

TABLE 1 | Skin viscoelasticity parameters measured using 2- and 6-mm probes in the low- and high-exposure groups.

	Low-exposure workers (mean ± SD)	High-exposure workers (mean ± SD)	Statistical test, *p*
(2 mm probe)			
R0 (skin pliability)	0.314 ± 0.107	0.219 ± 0.040	**0.0006**
R2 (gross elasticity)	0.811 ± 0.071	0.815 ± 0.065	> 0.9999
R5 (net elasticity)	1.058 ± 0.335	0.941 ± 0.173	0.6488
R6 (portion of viscoelasticity)	0.860 ± 0.364	0.869 ± 0.158	> 0.9999
R7 (immediate recovery)	0.557 ± 0.094	0.509 ± 0.107	0.6555
(6 mm probe)			
R0 (skin pliability)	0.735 ± 0.141	1.034 ± 0.134	**< 0.0001**
R2 (gross elasticity)	0.849 ± 0.068	0.796 ± 0.068	0.071
R5 (net elasticity)	1.001 ± 0.179	0.674 ± 0.127	**< 0.0001**
R6 (portion of viscoelasticity)	0.918 ± 0.237	0.598 ± 0.079	**< 0.0001**
R7 (immediate recovery)	0.523 ± 0.079	0.421 ± 0.080	**0.0007**

Note: Data are presented as the mean ± SD Two-way ANOVA (Geisser–Greenhouse correction) with Bonferroni's post hoc test was used to compare viscoelastic parameters (R0–R7) between exposure groups. Significant values (< 0.05) are shown in bold.

TABLE 2 | Skin color parameters (L*, a*, and b*) measured at the forehead and neck in the low and high-exposure groups.

	Low-exposure workers (mean ± SD)	High-exposure workers (mean ± SD)	Statistical test, *p*
(forehead)			
L*	55.65 ± 4.07	56.44 ± 2.53	> 0.9999
a*	10.19 ± 1.83	12.45 ± 1.97	**0.0012**
b*	16.51 ± 1.86	16.94 ± 1.66	> 0.9999
(neck)			
L*	60.64 ± 3.52	58.53 ± 3.44	0.1539
a*	7.69 ± 2.02	9.43 ± 2.34	**0.0432**
b*	19.02 ± 1.91	19.45 ± 0.96	0.9607

Note: Data are presented as the mean ± SD Two-way ANOVA (site × group, Geisser–Greenhouse correction) with Bonferroni's post hoc test was used for comparisons. L* indicates skin lightness, a* the red–green axis (erythema), and b* the yellow–blue axis (yellowness). Significant values (< 0.05) are shown in bold.

The levels of IFN-γ, CXCL10, and IL-1Ra were significantly higher in the high-exposure group than in the low-exposure group (Table 3). IL-10 showed a trend toward higher values in the high-exposure group ($p = 0.0600$) but did not reach statistical significance under the unpaired *t*-test. CCL3 also showed a nonsignificant trend ($p = 0.0719$). No significant differences were observed for IFN-α, IL-4, IL-8, or IL-1α.

3.3 | Molecular Responses to Fume Exposure in Human Keratinocytes

Cell viability was evaluated in HaCaT keratinocytes exposed to factory-derived welding fumes using the LDH release assay (Figure 5). To verify cytotoxicity at the exposure times applied in the reporter and gene expression assays, cell viability was measured after 6 and 24 h at concentrations of up to 100 μg/mL. No significant cytotoxicity was observed at 10 or 50 μg/mL, whereas only a modest reduction in cell viability was detected at 100 μg/mL after 24 h.

When HaCaT cells were exposed to welding fumes (10, 50, or 100 μg/mL), the ARE reporter assay exhibited significant activation at 100 μg/mL, at both 6 and 24 h. This indicated the transcriptional activation of the oxidative stress response pathway. The nuclear factor kappa B (NF-κB) reporter assay exhibited significant activation at 10–100 μg/mL at 24 h. This indicated the activation of inflammatory signaling pathways (Figure 6A–D).

mRNA expression analysis at 24 h revealed significant increases in the oxidative stress-related genes heme oxygenase 1 (HMOX-1) and NAD(P)H quinone dehydrogenase 1 (NQO-1) (Figure 7A,B). Consistent with these findings, TBARS levels (an indicator of lipid peroxidation) were significantly elevated at 100 μg/mL (Figure 7C).

Among inflammation-related genes, interleukin-6 (IL-6) mRNA expression showed a dose-dependent increase (Figure 7D), and matrix metalloproteinase (MMP) genes, including, MMP-3 and MMP-9 were significantly upregulated at higher concentrations (Figure 7E,F).

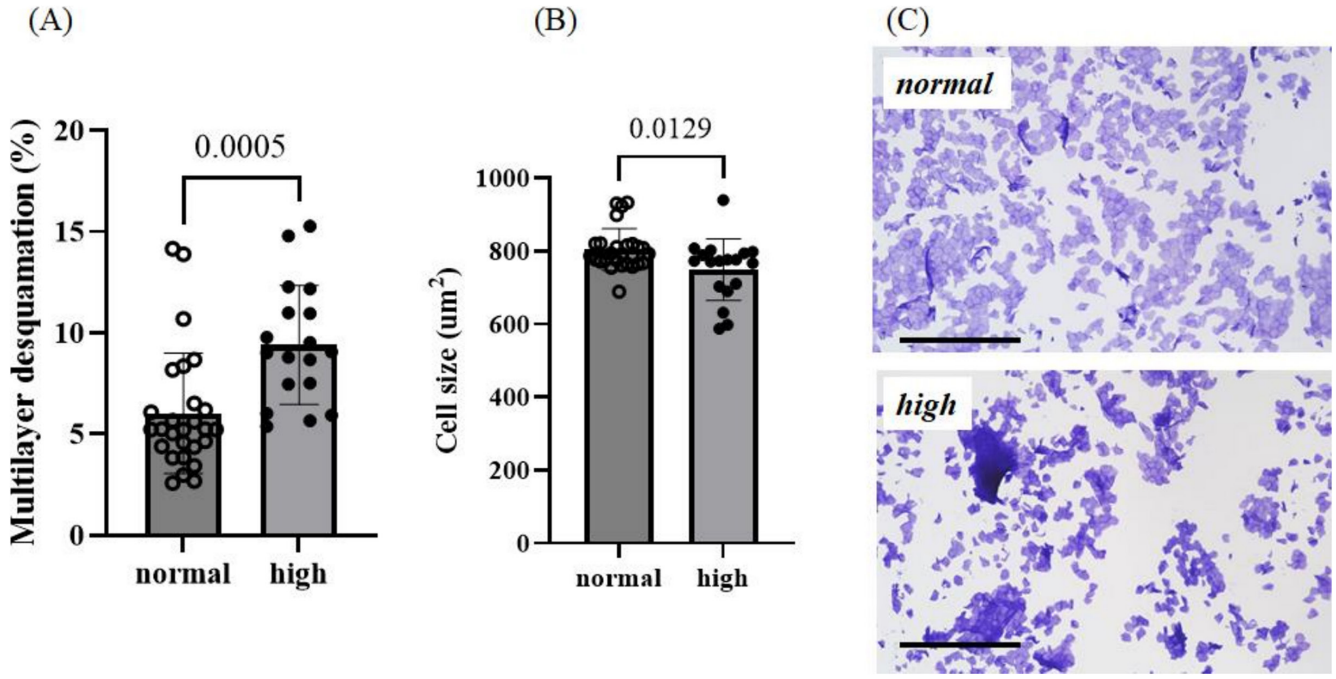

FIGURE 3 | Stratum corneum (SC) morphology in low- and high-exposure groups. (A) Multilayer desquamation score and (B) Corneocyte size (unpaired *t*-test). (C) Representative Brilliant Green-stained images of SC. Scale bars = 200 μm.

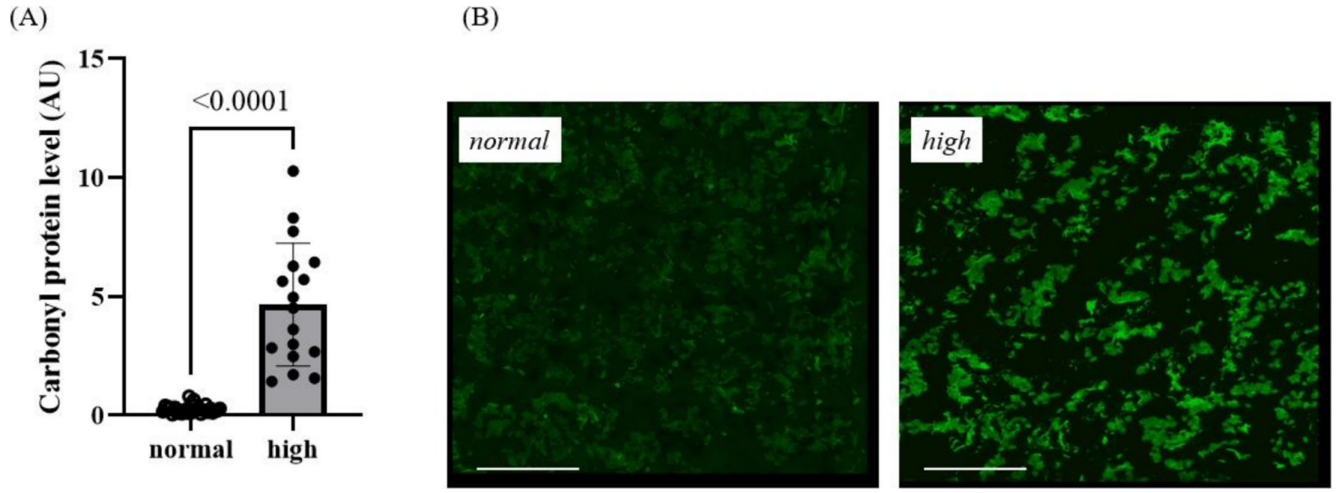

FIGURE 4 | Stratum corneum (SC) carbonylated protein levels in high- and low-exposure groups. (A) Quantification of carbonyl protein levels from fluorescence images (unpaired *t*-test). (B) Representative fluorescence images of SC samples from the low- and high-exposure groups. Scale bars = 200 μm.

At the protein level, IL-6 expression was significantly increased across all concentrations (Figures 7G), whereas MMP-3 and MMP-9 levels were elevated at 100 μg/mL (Figure 7H,I).

4 | Discussion

This study comprehensively assessed the effects of chronic exposure to PM2.5 (welding fumes) in factory (metal processing) and nonfactory environments on both skin conditions and cellular responses, using integrated in vivo and in vitro approaches. Environmental monitoring revealed that PM2.5 concentrations in both the welding area and its adjacent nonwelding area greatly exceeded the World Health Organization guideline value (Ma et al. 2025), thereby supporting our classification of participants into high- and low-exposure groups for skin assessments.

A primary strength of this study is that the in vivo and in vitro datasets, obtained at significantly different biological scales, converged on consistent trends across multiple indicators associated with oxidative stress and inflammatory responses. This concordance between cellular and clinical observations provides a coherent view of the cutaneous effects of environmental particulate exposure, from molecular pathways to functional and structural alterations. In particular, the occupational context provides a unique epidemiological perspective: workers are subjected to chronic and higher level PM2.5 exposures than those working in ambient environments; this allows detection of subtle but biologically meaningful changes. Simultaneously, limitations such as

TABLE 3 | Stratum corneum (SC) cytokine concentrations in the low- and high-exposure groups.

Cytokine	Low-exposure workers (mean ± SD)	High-exposure workers (mean ± SD)	Statistical test, *p*
IFNα	25.6 ± 9.9	34.0 ± 18.1	0.1296
IFNγ	88.5 ± 29.1	131.8 ± 34.6	**0.0065**
IL-10	24.2 ± 16.0	31.0 ± 21.0	0.0600
IL-4	24.1 ± 13.9	30.1 ± 17.9	0.2024
IL-8	48.9 ± 31.0	87.4 ± 124.2	0.3041
CXCL10	28.8 ± 13.9	45.3 ± 32.2	**0.0333**
CCL3	30.7 ± 24.9	37.2 ± 21.0	0.0719
IL-1Ra	5248.3 ± 4565.4	9501.0 ± 7722.4	**0.0232**
IL-1α	161.9 ± 134.9	181.9 ± 144.2	0.6360

Note: Data are presented as the mean ± SD Comparisons between low- and high-exposure groups were performed using an unpaired *t*-test (two-sided). Significant *p*-values (< 0.05) are shown in bold.

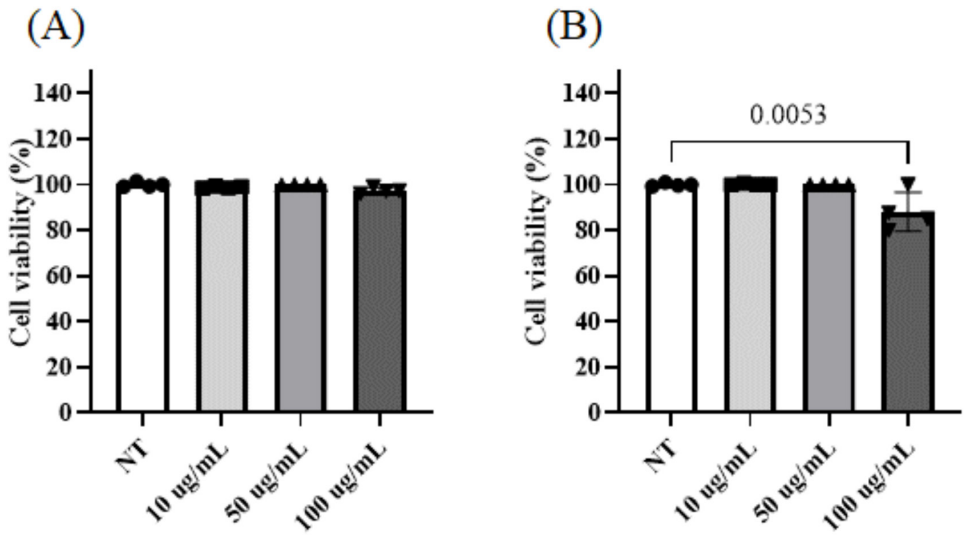

FIGURE 5 | Effects of welding fume exposure on HaCaT cell viability after 6 (A) and 24 h (B). Data are represented as the mean ± SEM ($n = 4$). (one-way ANOVA with Dunnett's test).

cross-sectional design, relatively small sample size, and seasonal differences in recruitment should be acknowledged. These factors may confound biomarker levels or obscure long-term trajectories, and thus, future longitudinal cohort studies are required.

In addition, methodological aspects of exposure assessment should be considered. In our previous work, we cross-validated particle count–based estimates of PM2.5 concentrations with gravimetric filter measurements and confirmed that the calculated mass values were in reasonable agreement with directly measured weights (Kono, Ishihara, et al. 2024). This prior validation supports the reliability of the exposure assessment approach employed in the present study, while acknowledging that both particle size distribution and density assumptions can still introduce a degree of estimation error.

Furthermore, to minimize the potential impact of seasonal variation in skin parameters, we included both the forehead and neck in our assessments, as the neck is reported to be less affected by environmental exposure and to exhibit lower TEWL compared to other facial sites (Leroy et al. 1998). Tape stripping for inflammatory markers was performed only at the forehead, as extending the procedure to multiple sites would have placed an excessive burden on participants. Importantly, the control group was assessed in July, when seasonal conditions would be expected to elevate inflammatory markers; however, the high-exposure group consistently showed stronger responses, including increased erythema (a*), elevated Th1-related chemokines, activation of the nuclear factor erythroid 2–related factor 2 (Nrf2)/ARE and NF-κB pathways, and reduced skin elasticity. These findings indicate that the primary results are unlikely to be explained by seasonal effects alone.

Next, considering these methodological aspects, we evaluated oxidative stress responses; in vivo analyses revealed significantly increased levels of carbonylated proteins in the SC of the high-exposure group, together with alterations in specific viscoelastic parameters. In particular, significant changes

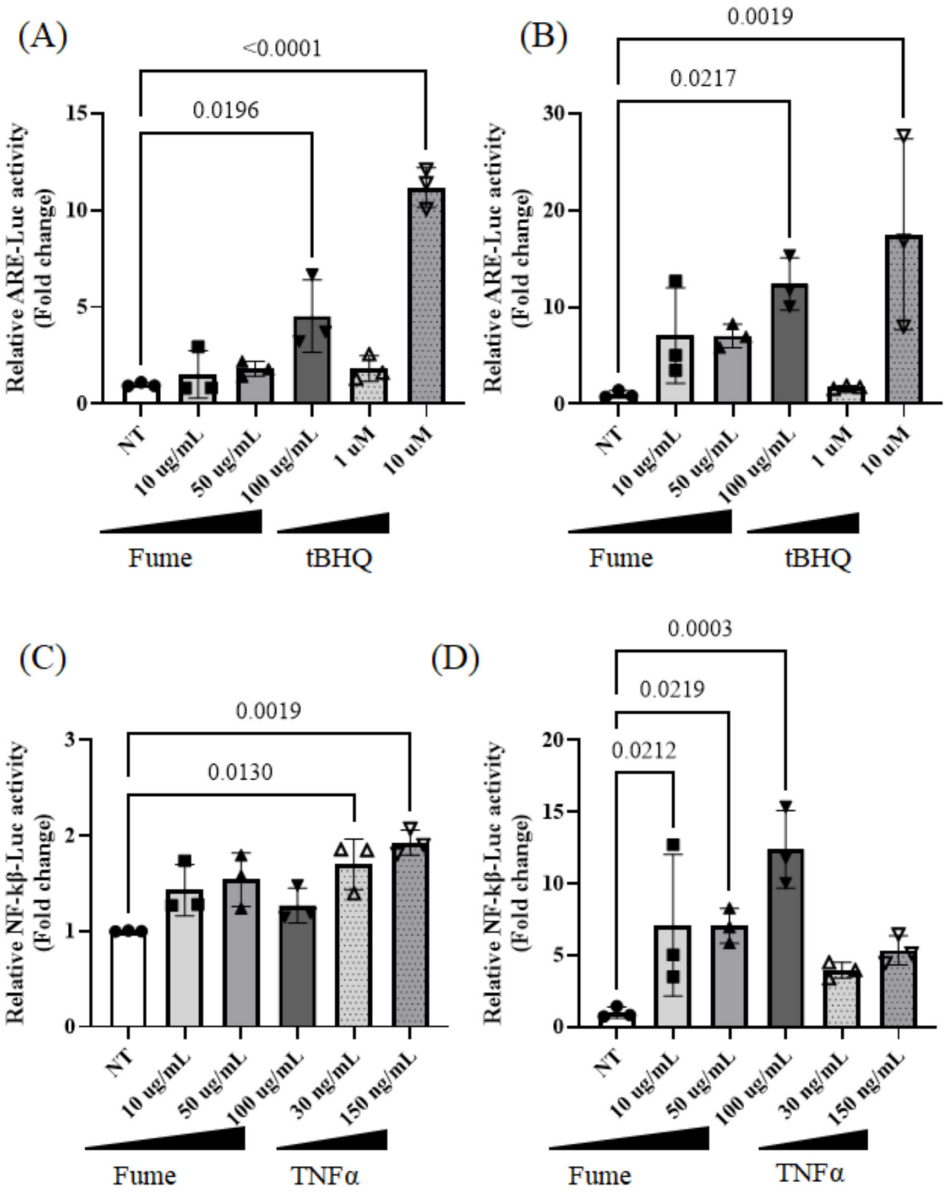

FIGURE 6 | Effects of welding fume exposure on antioxidant response element (ARE) and nuclear factor kappa B (NF-κB)-mediated reporter activity in HaCaT cells. HaCaT cells were transfected with the NF-κB-Luc (A, B) or ARE-Luc (C, D) and each compound was treated for 6 (A,C) or 24 h (B,D). Data are represented as the mean ± SEM ($n = 3$ biological replicates). (two-way ANOVA with Tukey's post hoc test).

were observed in R0 (skin pliability) and R7 (immediate recovery), whereas other parameters showed no consistent differences between the exposure groups. These findings indicate that welding fume exposure may selectively impair certain components of skin elasticity, instead of causing a generalized reduction in viscoelastic properties. These alterations indicate that oxidative damage extends to structural alterations and disrupted epidermal turnover, resembling skin aging and dryness (Izutsu-Matsumoto et al. 2025). Consistent with these observations, in vitro experiments revealed increased ARE reporter activity and upregulation of antioxidant genes (NQO-1 and HMOX-1), confirming the activation of the Nrf2/ARE oxidative stress response pathway (Yue et al. 2022). Oxidative stress impairs barrier function (Li et al. 2017; Kim et al. 2023). Notably, our findings support the association between barrier impairment and cellular oxidative responses. In contrast, MMP-1 was not significantly upregulated, despite its association with PM2.5- or UV-induced dermal matrix degradation (Herath et al. 2022; Jang et al. 2023). Possible explanations include the predominantly metallic composition of welding fumes that have a relatively low polycyclic aromatic hydrocarbon (PAH) content, and the likelihood that chronic, low-level exposure induces these enzymes less strongly than acute damage (Dijkhoff et al. 2020). In addition, dermal-level alterations may require longer exposure durations than those observed in this cross-sectional study. The elemental composition data (Table S1) further support this interpretation, showing that welding-derived PM2.5 is markedly enriched in transition metals such as Fe and Mn compared with ambient PM2.5 collected in urban areas of Japan (Fukuoka and Yokohama). These metals are potent catalysts of ROS formation, which may preferentially activate oxidative stress–responsive pathways (such as Nrf2/ARE) instead of aryl hydrocarbon receptor (AhR)-mediated transcription of MMP-1, thereby explaining the differential MMP expression

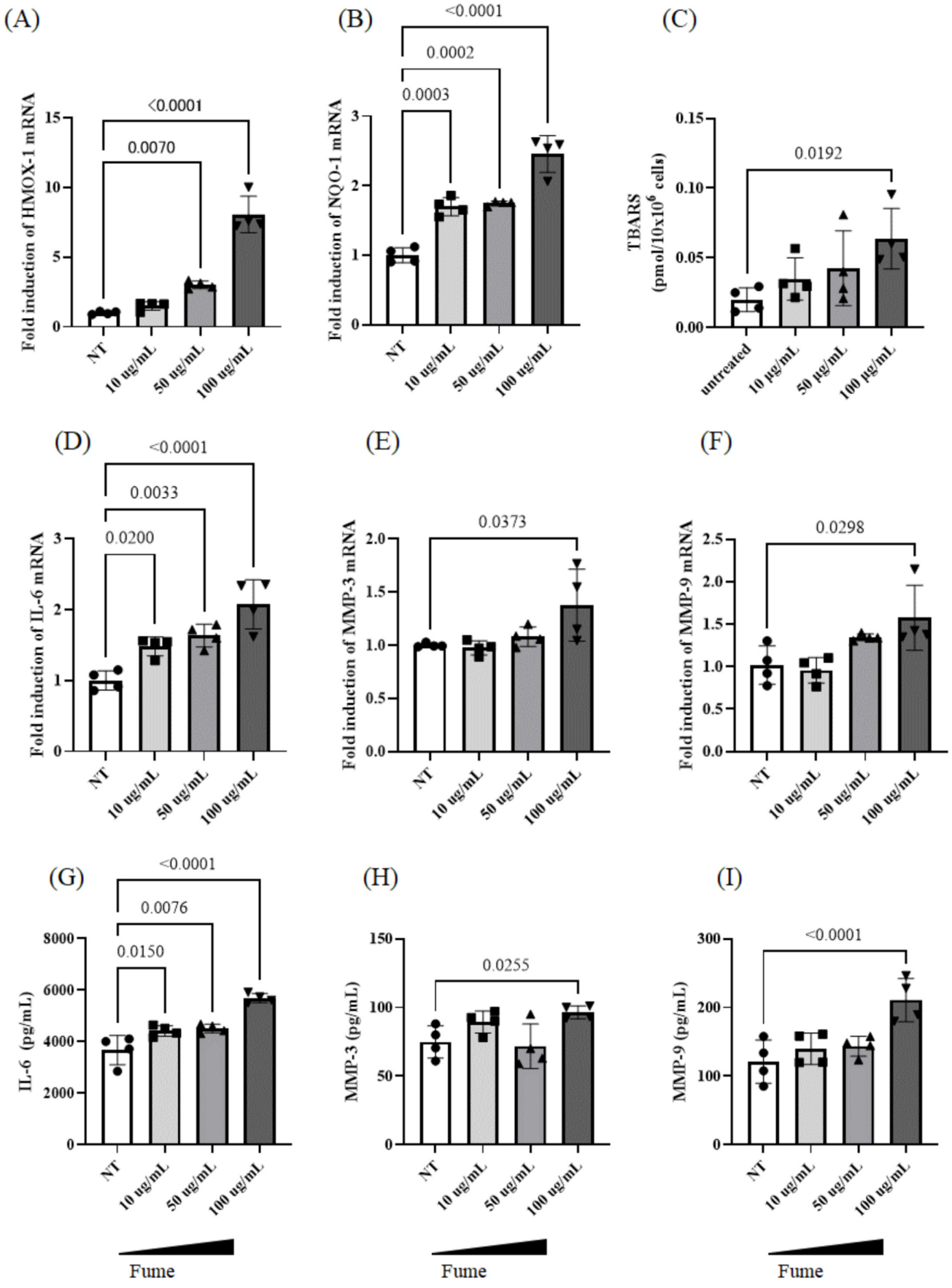

FIGURE 7 | Legend on next page.

FIGURE 7 | Effects of welding fume exposure on oxidative stress and inflammatory responses in HaCaT cells. HaCaT keratinocytes were exposed to welding fume suspensions (10, 50, or 100 μg/mL) for 24 h, except for lipid peroxidation analysis (6 h). mRNA expression levels of heme oxygenase-1 (HMOX-1) (A), NAD(P)H quinone dehydrogenase 1 (NQO-1) (B), interleukin-6 (IL-6) (D), matrix metalloproteinase-3 (MMP-3) (E), and matrix metalloproteinase-9 (MMP-9) (F) were quantified using real-time PCR and normalized to β-actin. Lipid peroxidation was evaluated by quantifying thiobarbituric acid-reactive substances (TBARS) (C) in cell homogenates. Protein levels of IL-6 (G), MMP-3 (H), and MMP-9 (I) in the culture supernatants were determined using a multiplex immunoassay. Data are presented as the mean ± SEM ($n = 4$) (two-way ANOVA with Dunnett's post hoc test).

profile observed here. This discrepancy may also reflect fundamental mechanistic differences between welding fumes and traffic-related PM2.5. Traffic-derived particles are enriched in PAHs and carbonaceous fractions, particularly at roadside sites (Shams Solari et al. 2022), which can activate AhR- dependent signaling and drive MMP-1 expression in dermal fibroblasts (Ono et al. 2013). In contrast, welding fumes consist predominantly of metal oxides (e.g., Fe, Mn, and Zn) (Li et al. 2004) that generate reactive oxygen species (ROS) and oxidative stress, with prominent Nrf2/ARE activation (Graczyk et al. 2016), but not consistently inducing MMP-1. Consistent with this mechanism, our results revealed upregulation of MMP-3 and MMP-9 at high-exposure concentrations, together with signs of reduced dermal viscoelasticity, indicating that metal-oxide–driven oxidative stress may promote extracellular matrix remodeling through alternative MMPs instead of MMP-1. Moreover, PAHs are highly lipophilic and can penetrate across the epidermal barrier (Bocheva et al. 2023), potentially reaching deeper skin layers, whereas inorganic metal-oxide particles generally exhibit more limited penetration across intact SC (Bocheva et al. 2023). These compositional and penetrative differences plausibly underlie the weaker induction of MMP-1 observed here. Regarding inflammatory responses, in vivo measurements revealed increased skin redness (a* values) and elevated levels of the Th1-associated cytokines IFN-γ and CXCL10 in the high-exposure group. In vitro findings revealed NF-κB activation and enhanced IL-6 expression, supporting the involvement of NF-κB–mediated chronic inflammation (Mao et al. 2025). CXCL10 contributes to Th1 immune polarization and the recruitment of monocytes and T cells (Yoneyama et al. 2002; Griffith et al. 2014), and its upregulation aligns with clinically observed erythema. Notably, IL-1Ra levels were also significantly increased, whereas IL-10 showed only a nonsignificant trend and CCL3 displayed a similar trend without reaching significance, and IL-1α levels remained unchanged between groups. IL-1Ra is an endogenous antagonist that suppresses IL-1–mediated inflammation and functions as a negative feedback mechanism under chronic stimulation (Martin et al. 2021). Seasonal factors may have affected IL-1α results because the low-exposure group was assessed during summer, when transient UV-induced IL-1α increases may elevate baseline values.

Although cytokine levels exhibited inter-individual variability, a selective pattern of cytokine alterations—particularly increases in IFN-γ, CXCL10, and IL-1Ra—supports the presence of an exposure-related inflammatory/immune-activation signature, rather than a uniform cytokine-wide shift. Regarding pigmentation, recent studies have associated PM2.5 exposure with increased melanogenesis and exacerbation of postinflammatory hyperpigmentation (Yang et al. 2022; Ding et al. 2017). In this study, the increase in a* values was consistent with the potential pigmentation risk, highlighting the cosmetic and clinical concerns.

Notably, welding fumes are not restricted to PM2.5-sized particles. Our previous analyses revealed that they contain abundant ultrafine particles (< 0.1 μm) enriched with transition metals such as Fe and Mn (Kono, Ishihara, et al. 2024). These compositional features may amplify oxidative stress and inflammatory responses beyond those observed with larger PM2.5 fractions. The present study, therefore, likely underestimates the full spectrum of cutaneous risks associated with occupational fume exposure, as ultrafine particles are more capable of penetrating skin appendages and reaching the dermal vasculature. Collectively, both PM2.5 and smaller ultrafine fractions should be considered as key contributors to welding fume-induced skin toxicity.

From a toxicological perspective, these findings emphasize the need to consider the skin as a target organ for environmental pollutants. The skin is the largest organ of the human body and plays a pivotal role as a physical and immunological barrier (Kupper and Fuhlbrigge, 2004). In this study, we also considered endogenous factors that can affect skin barrier function.

Aging is known to decrease barrier integrity through reductions in SC lipids and natural moisturizing factors (Ganceviciene et al. 2012). Hormonal status is another important determinant of skin barrier properties. Estrogen deficiency impairs SC integrity by reducing epidermal lipids and natural moisturizing factors (Rzepecki et al. 2019). In this study, we restricted participants to male workers to minimize the influence of estrogen fluctuations and age-related variability, thereby providing a clearer context for evaluating the direct impact of occupational PM2.5 exposure on the skin. However, this male-only design inevitably limits the generalizability of our findings, as female skin barrier function is strongly influenced by estrogen levels (Rzepecki et al. 2019; Ganceviciene et al. 2012). Moreover, testosterone absorption has been reported to depend on barrier integrity (Brackin et al. 2024), highlighting the complex interplay between sex hormones and the epidermal barrier. These observations indicate that both endogenous hormonal factors and barrier conditions can mutually influence hormone penetration and biological responses in the skin. Consequently, the barrier impairment observed in this study can be interpreted as primarily attributable to exogenous factors such as welding fume exposure, although residual contributions from intrinsic physiological factors cannot be entirely excluded. Therefore, future studies including female participants are required to confirm the sex-specific relevance of these findings.

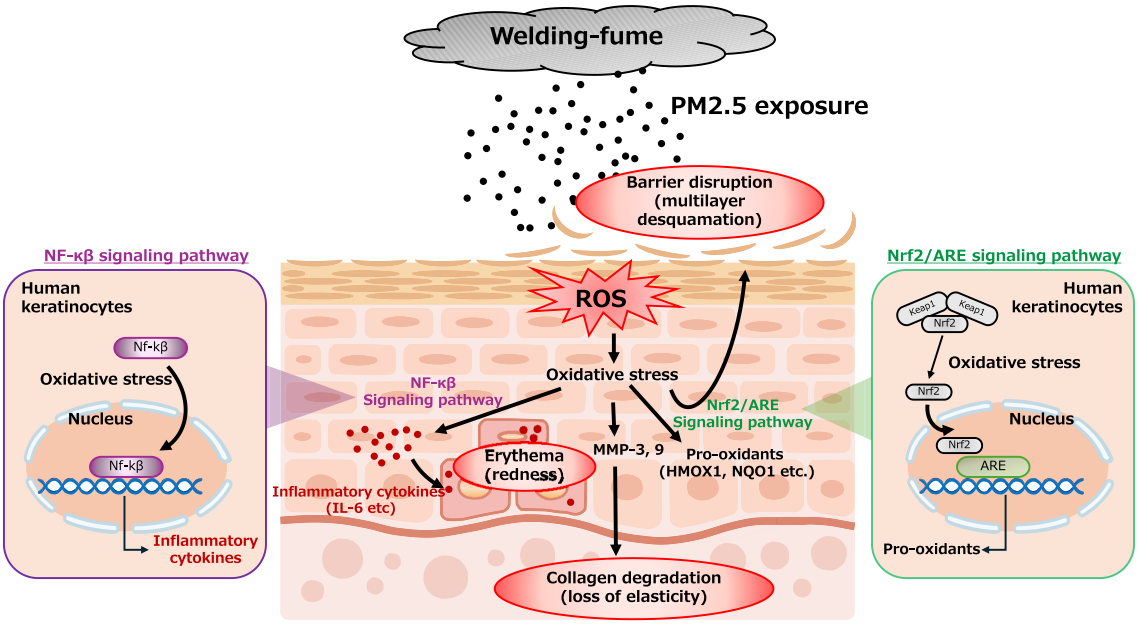

FIGURE 8 | Proposed mechanism of welding fume-induced skin responses. Occupational exposure to welding fume PM2.5 containing Fe, Mn, and Zn induces excessive generation of reactive oxygen species (ROS), leading to oxidative stress. The resulting activation of NF-κB and Nrf2/ARE pathways triggers inflammatory cytokine release, upregulation of MMP-3 and MMP-9, and antioxidant responses. These molecular events collectively result in barrier disruption (multilayer desquamation), erythema (redness), and collagen degradation (loss of elasticity).

Although PM2.5 particles are generally considered too large to readily penetrate intact skin (Paik et al. 2024), chronic external insults, such as long-term exposure to oxidative and inflammatory stressors, can weaken barrier integrity. Under such conditions, particulate matter may gain enhanced access into deeper layers of the SC, exacerbating toxicological effects (Paik et al. 2024). This dynamic interaction between barrier disruption and pollutant penetration indicates that chronic occupational exposures could amplify cutaneous toxicity in a self-perpetuating cycle. This creates a cycle in which barrier dysfunction increases vulnerability to further environmental insults. This cycle has important implications for occupational toxicology, as it expands the traditional focus from respiratory and systemic toxicity to include cutaneous endpoints.

In summary, both in vivo and in vitro approaches revealed that PM2.5 exposure induces oxidative stress and inflammatory responses in the skin. Activation of the Nrf2/ARE and NF-κB pathways was closely associated with structural (elasticity loss and corneocyte alterations) and visible (erythema) alterations, representing the primary strength of our integrated methodology.

Although the number of subjects was relatively small (high-exposure group: $n = 18$, low-exposure group: $n = 28$), significant differences in skin parameters were observed, likely because of the clear contrast in occupational exposure sources. Therefore, this study provides preliminary evidence linking factory-derived PM2.5 exposure to skin alterations. Building upon these findings, we propose a mechanistic model in which welding-fume exposure impairs skin function via ROS-mediated activation of the Nrf2/ARE and NF-κB pathways (Figure 8).

Future research should further address particle composition, exposure route, dose, and inter-individual variability in occupational cohorts, to clarify causal relationships and strengthen toxicological frameworks for worker health protection.

5 | Conclusions

This study reveals that exposure to factory-derived PM2.5, particularly welding fumes, induces cutaneous toxicity characterized by oxidative stress, inflammation, and barrier dysfunction. The integration of human epidemiological data and keratinocyte-based assays highlights the skin as a relevant target organ in occupational toxicology. These findings broaden the scope of occupational health by incorporating skin as a key endpoint, provide a basis for recognizing skin health within exposure evaluations, and highlight the need for preventive strategies to mitigate pollution-induced skin damage in worker populations.

Acknowledgments

The authors thank Mr. Hidefumi Ikeda of Mandom Corporation and Dr. Yukiko Izutsu-Matsumoto of CIEL Co. Ltd. for their helpful discussions regarding the design of the epidemiological study evaluation and statistical analysis.

Conflicts of Interest

The authors declare no conflicts of interest.

Data Availability Statement

The data that support the findings of this study are available on request from the corresponding author. The data are not publicly available due to privacy or ethical restrictions.

References

Bocheva, G., R. M. Slominski, and A. T. Slominski. 2023. "Environmental Air Pollutants Affecting Skin Functions With Systemic Implications." *International Journal of Molecular Sciences* 24, no. 13: 10502. https://doi.org/10.3390/ijms241310502.

Brackin, T., H. Gayes, I. Johnson, D. Fox, and C. Roper. 2024. "Skin Barrier Function for Regulatory Skin Absorption Tests and Effects on Testosterone and Sucrose Absorption." *Toxicology In Vitro* 95: 105735. https://doi.org/10.1016/j.tiv.2023.105735.

Chan, F. Y., C. P. Chio, T. H. Yuan, et al. 2025. "Association Between PM2.5 and Skin Redness Features in Taiwan." *PLOS Glob Public Health* 5, no. 3: e0004357. https://doi.org/10.1371/journal.pgph.0004357.

Dijkhoff, I. M., B. Drasler, B. B. Karakocak, et al. 2020. "Impact of Airborne Particulate Matter on Skin: A Systematic Review From Epidemiology to In Vitro Studies." *Particle and Fibre Toxicology* 17, no. 1: 35. https://doi.org/10.1186/s12989-020-00366-y.

Ding, A., Y. Yang, Z. Zhao, et al. 2017. "Indoor PM(2.5) Exposure Affects Skin Aging Manifestation in a Chinese Population." *Scientific Reports* 7, no. 1: 15329. https://doi.org/10.1038/s41598-017-15295-8.

Ei, Z. Z., A. Mutirangura, and P. Chanvorachote. 2025. "Secretome From HMGB1 Box A-Over-Expressing Adipose-Derived Stem Cells Shows Potential for Skin Rejuvenation by Senescence Reversal in PM2.5-Induced Senescence Cells via Stem Cell Induction." *In Vivo* 39, no. 2: 766–777. https://doi.org/10.21873/invivo.13881.

Fujimoto, Y., Y. Yuri, Y. Kato, S. Kinoshita, and H. Tamiya. 2023. "Intra- and Inter-Rater Reliabilities of Skin Mechanical Properties Measured in Healthy Individuals Using Skin Elasticity Meter." *Annals of Medicine* 55, no. 2: 2279747. https://doi.org/10.1080/07853890.2023.2279747.

Ganceviciene, R., A. I. Liakou, A. Theodoridis, E. Makrantonaki, and C. C. Zouboulis. 2012. "Skin Anti-Aging Strategies." *Dermato-Endocrinology* 4, no. 3: 308–319. https://doi.org/10.4161/derm.22804.

Graczyk, H., S. Linder, S. Deslarzes, et al. 2016. "Time-Course Changes of Oxidative Stress Biomarkers in Exhaled Breath Condensate, Plasma, and Urine of Apprentice Welders Exposed to TIG Welding Fumes." *Particle and Fibre Toxicology* 13: 31. https://doi.org/10.1186/s12989-016-0149-7.

Griffith, J. W., C. L. Sokol, and A. D. Luster. 2014. "Chemokines and Chemokine Receptors: Positioning Cells for Host Defense and Immunity." *Annual Review of Immunology* 32: 659–702. https://doi.org/10.1146/annurev-immunol-032713-120145.

Herath, H., M. J. Piao, K. A. Kang, et al. 2022. "Hesperidin Exhibits Protective Effects Against PM2.5-Mediated Mitochondrial Damage, Cell Cycle Arrest, and Cellular Senescence in Human HaCaT Keratinocytes." *Molecules* 27, no. 15. https://doi.org/10.3390/molecules27154800.

Hu, R., X. Y. Xie, S. K. Xu, et al. 2017. "PM(2.5) Exposure Elicits Oxidative Stress Responses and Mitochondrial Apoptosis Pathway Activation in HaCaT Keratinocytes." *Chinese Medical Journal* 130, no. 18: 2205–2214. https://doi.org/10.4103/0366-6999.212942.

Huang, C. H., S. C. Chen, Y. C. Wang, C. F. Wang, C. H. Hung, and S. S. Lee. 2022. "Detrimental Correlation Between Air Pollution With Skin Aging in Taiwan Population." *Medicine (Baltimore)* 101, no. 31: e29380. https://doi.org/10.1097/MD.0000000000029380.

Huls, A., A. Vierkotter, W. Gao, et al. 2016. "Traffic-Related Air Pollution Contributes to Development of Facial Lentigines: Further Epidemiological Evidence From Caucasians and Asians." *Journal of Investigative Dermatology* 136, no. 5: 1053–1056. https://doi.org/10.1016/j.jid.2015.12.045.

Ishihara, Y., T. Haarmann-Stemmann, N. Y. Kado, and C. F. A. Vogel. 2019. "Interleukin 33 Expression Induced by Aryl Hydrocarbon Receptor in Macrophages." *Toxicological Sciences* 170, no. 2: 404–414. https://doi.org/10.1093/toxsci/kfz114.

Ishihara, Y., S. Hama, M. Watanabe, S. Danjo, Y. Nakamura, and K. Itoh. 2012. "Effects of Sulfaphenazole After Collagenase-Induced Experimental Intracerebral Hemorrhage in Rats." *Biological & Pharmaceutical Bulletin* 35, no. 10: 1849–1853. https://doi.org/10.1248/bpb.b12-00525.

Iwai, I., K. Shimadzu, Y. Kobayashi, T. Hirao, and T. Etou. 2010. "Increased Carbonyl Protein Level in the Stratum Corneum of Inflammatory Skin Disorders: A Non-Invasive Approach." *Journal of Dermatology* 37, no. 8: 693–698. https://doi.org/10.1111/j.1346-8138.2010.00867.x.

Izutsu-Matsumoto, Y., Y. Okano, H. Masaki, Y. Tokudome, and T. Iwabuchi. 2025. "Effect of Low Humidity on the Barrier Functions of Keratinocytes in a Reconstructed Human Epidermal Model." *International Journal of Cosmetic Science* 47, no. 3: 523–534. https://doi.org/10.1111/ics.13048.

Jang, H. Y., G. B. Kim, J. M. Kim, et al. 2023. "Fisetin Inhibits UVA-Induced Expression of MMP-1 and MMP-3 Through the NOX/ROS/MAPK Pathway in Human Dermal Fibroblasts and Human Epidermal Keratinocytes." *International Journal of Molecular Sciences* 24, no. 24. https://doi.org/10.3390/ijms242417358.

Kim, H. B., M. G. Choi, B. Y. Chung, et al. 2023. "Particulate Matter 2.5 Induces the Skin Barrier Dysfunction and Cutaneous Inflammation via AhR- and T Helper 17 Cell-Related Genes in Human Skin Tissue as Identified via Transcriptome Analysis." *Experimental Dermatology* 32, no. 4: 547–554. https://doi.org/10.1111/exd.14724.

Kono, M., N. Ishihara, T. Nakane, et al. 2024. "Enhancement of Keratinocyte Survival and Migration Elicited by Interleukin 24 Upregulation in Dermal Microvascular Endothelium Upon Welding-Fume Exposure." *Journal of Toxicology and Environmental Health. Part A* 87, no. 19: 792–810. https://doi.org/10.1080/15287394.2024.2372403.

Kono, M., T. Okuda, N. Ishihara, et al. 2023. "Chemokine Expression in Human 3-Dimensional Cultured Epidermis Exposed to PM2.5 Collected by Cyclonic Separation." *Toxicology Research* 39, no. 1: 1–13. https://doi.org/10.1007/s43188-022-00142-4.

Kono, M., M. Takaishi, T. Okuda, M. Fujihara, S. Noguchi, and Y. Ishihara. 2024. "A Simple Air-Liquid Interface Exposure System for Exposing Cultured Human 3D Epidermis and Cornea to PM2.5 Collected Through Cyclonic Separation." *Journal of Toxicological Sciences* 49, no. 2: 61–68. https://doi.org/10.2131/jts.49.61.

Kupper, T. S., and R. C. Fuhlbrigge. 2004. "Immune Surveillance in the Skin: Mechanisms and Clinical Consequences." *Nature Reviews. Immunology* 4, no. 3: 211–222. https://doi.org/10.1038/nri1310.

Leroy, T., C. Geveaux, J. Crucq, L. F. A. Douven, and D. Van Neste. 1998. "The Face and Neck: Regional Variation in Skin Barrier Function and Reactivity." *Skin Research and Technology* 4, no. 4: 205–212. https://doi.org/10.1111/j.1600-0846.1998.tb00112.x.

Li, G. J., L. L. Zhang, L. Lu, P. Wu, and W. Zheng. 2004. "Occupational Exposure to Welding Fume Among Welders: Alterations of Manganese, Iron, Zinc, Copper, and Lead in Body Fluids and the Oxidative Stress Status." *Journal of Occupational and Environmental Medicine* 46, no. 3: 241–248. https://doi.org/10.1097/01.jom.0000119769.10648.20.

Li, Q., Z. Kang, S. Jiang, et al. 2017. "Effects of Ambient Fine Particles PM(2.5) on Human HaCaT Cells." *International Journal of Environmental Research and Public Health* 14, no. 1. https://doi.org/10.3390/ijerph14010072.

Ma, X., L. Morawska, B. Zou, et al. 2025. "Towards Compliance With the 2021 WHO Air Quality Guidelines: A Comparative Analysis of PM(2.5) Trends in Australia and China." *Environment International* 198: 109378. https://doi.org/10.1016/j.envint.2024.109378.

Mao, H., X. Zhao, and S. C. Sun. 2025. "NF-kappaB in Inflammation and Cancer." *Cellular & Molecular Immunology* 22, no. 8: 811–839. https://doi.org/10.1038/s41423-025-01310-w.

Martin, P., J. D. Goldstein, L. Mermoud, A. Diaz-Barreiro, and G. Palmer. 2021. "IL-1 Family Antagonists in Mouse and Human Skin Inflammation." *Frontiers in Immunology* 12: 652846. https://doi.org/10.3389/fimmu.2021.652846.

Ono, Y., K. Torii, E. Fritsche, Y. Shintani, E. Nishida, and C. F. A. Vogel. 2013. "Role of the Aryl Hydrocarbon Receptor in Tobacco Smoke-Induced MMP-1 Expression in Human Fibroblasts and Keratinocytes." *Experimental Dermatology* 22, no. 4: 349–353. https://doi.org/10.1111/exd.12145.

Paik, K., J. I. Na, C. H. Huh, and J. W. Shin. 2024. "Particulate Matter and Its Molecular Effects on Skin: Implications for Various Skin Diseases." *International Journal of Molecular Sciences* 25, no. 18. https://doi.org/10.3390/ijms25189888.

Piao, M. J., M. J. Ahn, K. A. Kang, et al. 2018. "Particulate Matter 2.5 Damages Skin Cells by Inducing Oxidative Stress, Subcellular Organelle Dysfunction, and Apoptosis." *Archives of Toxicology* 92, no. 6: 2077–2091. https://doi.org/10.1007/s00204-018-2197-9.

Ryu, H. S., Y. H. Joo, S. O. Kim, K. C. Park, and S. W. Youn. 2008. "Influence of Age and Regional Differences on Skin Elasticity as Measured by the Cutometer." *Skin Research and Technology* 14, no. 3: 354–358. https://doi.org/10.1111/j.1600-0846.2008.00302.x.

Rzepecki, A. K., J. E. Murase, R. Juran, S. G. Fabi, and B. N. McLellan. 2019. "Estrogen-Deficient Skin: The Role of Topical Therapy." *International Journal of Women's Dermatology* 5, no. 2: 85–90. https://doi.org/10.1016/j.ijwd.2019.01.001.

Shams Solari, M., A. H. Mahvi, M. Alimohammadi, M. Alimohammadi, and M. G. Ghozikali. 2022.

Tanaka, M., T. Okuda, K. Itoh, et al. 2023. "Polycyclic Aromatic Hydrocarbons in Urban Particle Matter Exacerbate Movement Disorder After Ischemic Stroke via Potentiation of Neuroinflammation." *Particle and Fibre Toxicology* 20, no. 1: 6. https://doi.org/10.1186/s12989-023-00517-x.

Wang, C., Y. Tu, Z. Yu, and R. Lu. 2015. "PM2.5 and Cardiovascular Diseases in the Elderly: An Overview." *International Journal of Environmental Research and Public Health* 12, no. 7: 8187–8197. https://doi.org/10.3390/ijerph120708187.

Woo, M. S., K. J. Moon, H. Y. Jung, et al. 2014. "Comparison of Skin Elasticity Test Results From the Ballistometer((R)) and Cutometer((R))." *Skin Research and Technology* 20, no. 4: 422–428. https://doi.org/10.1111/srt.12134.

Yang, X., F. Peng, J. Huang, Z. Chen, and J. Zhang. 2022. "Particulate Matter 2.5 Induced Hyperpigmentation in Reconstructed Human Epidermis Model (MelaKutis(R))." *Chinese Medical Journal* 135, no. 4: 502–504. https://doi.org/10.1097/CM9.0000000000001934.

Yoneyama, H., S. Narumi, Y. Zhang, et al. 2002. "Pivotal Role of Dendritic Cell-Derived CXCL10 in the Retention of T Helper Cell 1 Lymphocytes in Secondary Lymph Nodes." *Journal of Experimental Medicine* 195, no. 10: 1257–1266. https://doi.org/10.1084/jem.20011983.

Yu, H., Y. Lin, Y. Zhong, et al. 2022. "Impaired AT2 to AT1 Cell Transition in PM2.5-Induced Mouse Model of Chronic Obstructive Pulmonary Disease." *Respiratory Research* 23, no. 1: 70. https://doi.org/10.1186/s12931-022-01996-w.

Yue, D., Q. Zhang, J. Zhang, et al. 2023. "Diesel Exhaust PM2.5 Greatly Deteriorates Fibrosis Process in Pre-Existing Pulmonary Fibrosis via Ferroptosis." *Environment International* 171: 107706. https://doi.org/10.1016/j.envint.2022.107706.

Yue, Q., X. Chen, J. Gao, Q. Gong, J. Shi, and F. Li. 2022. "Dendrobine Protects HACAT Cells From H(2)O(2)-Induced Oxidative Stress and Apoptosis Damage via Nrf2/Keap1/ARE Signaling Pathway." *Toxicology and Applied Pharmacology* 454: 116217. https://doi.org/10.1016/j.taap.2022.116217.

Supporting Information

Additional supporting information can be found online in the Supporting Information section. **Table S1:** Metal contents in welding fumes and PM2.5 collected in Japan.